Strojniški vestnik - Journal of Mechanical Engineering 68(2022)12, 735-745
DOI:10.5545/sv-jme.2022.306
Original Scientific Paper
Received for review: 2022-08-01
Received revised form: 2022-11-10
Accepted for publication: 2022-11-28

Investigation of Laser Ablative Micromachining of Al/TiB_2 Nanocomposite

Pratheesh Kumar Manikandan Rajam* – Jayakrishnan Nampoothiri
PSG College of Technology, Department of Production Engineering, India

Laser beam machining (LBM) is used to machine a variety of materials economically and to obtain the required quality metrics. The quality of the surface finish of laser-machined components is affected by the improper selection of process parameters during machining. In this paper, microchannels were machined on Al/TiB_2 nanocomposite using an Nd: YAG laser system. An atomic force microscope was used to obtain the surface roughness of microchannels. The aim of this process is to identify the influence of the individual and interactive effect of the process parameters on the surface roughness of the microchannels and to identify the optimum combination of the process parameters for minimum surface roughness. Taguchi's L9 orthogonal array-based Design of Experiment (DoE) was implemented to conduct the experimental study. A statistical analysis of the results was performed for the experimental data. The results are presented in detail.
Keywords: Laser micromachining, surface roughness, nanocomposite, parameter optimization, Taguchi methodology, Nd: YAG Laser

Highlights
- *Al/TiB_2 nanocomposite processing, characterization, and laser micromachining of Al/TiB_2 is explained in detail.*
- *Measurement of surface roughness (Ra) of microchannels using atomic force microscope and the optimum combination of the LBM parameters is determined.*
- *Analysis of the influence of the interaction effect of the laser-machining process parameters on Ra is presented.*

0 INTRODUCTION

Unconventional machining processes have gained a significant amount of research attention owing to their ruggedness and efficiency. Such machining processes are being utilized to machine high-strength materials with complex shapes in an easy manner. The conventional machining processes require cutting tools harder than the workpiece. These processes also result in the poor surface finish of the workpiece at the micro level due to abrasion. Advanced ceramic materials, such as aluminium oxide, zirconia, aluminium titanate, magnesium oxide, and silicon carbide have a variety of applications due to their thermo-physical and mechanical characteristics [1]. The laser can be utilized to cut such high-strength alloys to obtain the required shape and dimension. The concentrated energy of the laser beam is highly intended to melt high-strength materials due to its high-power density [2]. Laser beam machining (LBM) process is preferred over the other unconventional machining processes owing to its high ablation rate and the ability to yield a good surface finish. The laser is used for generating complex 2D and 3D patterns at micromachining domains [3] to [5]. The schematic diagram of a typical laser beam machining system is shown in Fig. 1. The scope to explore the laser micromachining of anisotropic metal matrix composites is very high.

Kibria et al. [6] machined micro-grooves on aluminium oxide ceramic to study the effect of successive spot and circumferential overlap of the laser beam on the roughness of the machined surface. Different spot overlaps have been used along with the other input parameters. The results showed that surface roughness decreases with the increase of both the overlap factors. Yue and Lau [7] investigated the pulsed laser cutting of an Al-Li/SiC metal matrix composite and concluded that it is possible to minimize the heat-affected zone (HAZ) and improve the machined surface quality with proper control of process parameters. It was found that proper control over the machining parameters is required to improve the surface finish and minimize the HAZ.

Qiao et al. [8] used a Nd: DPSS laser system with a repetition frequency of 20 kHz to 120 kHz and a maximum power of 25 W to investigate the effects of water jet guided laser micro-machining on surface topography, greatest aspect ratio evolution, and kerf edge fluctuations. The experimental findings showed no signs of oxidation or cracks on the kerf edge or other surfaces. The kerf aspect ratio ranged up to 12.7, indicating that the kerf is extremely steep. A form of water-conducting laser processing technique was developed by Zhihe et al. [9]. The basis of laser water-jet coupling technology was used to construct a set of water-conducting laser processing system. Studies on water-conducting laser processing were conducted on a variety of metal materials. The work

*Corr. Author's Address: PSG College of Technology, Coimbatore 641004, India, mrpratheesh@gmail.com

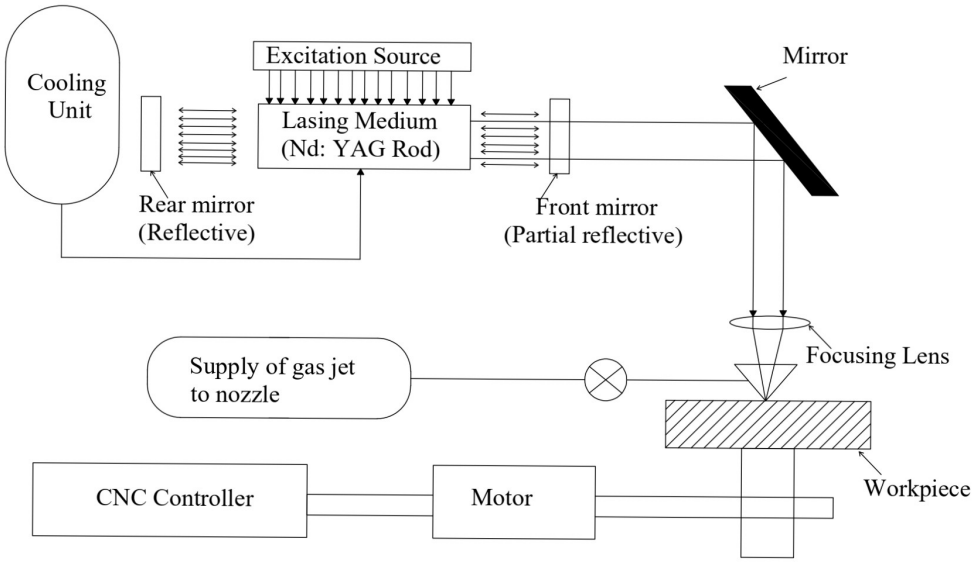

Fig. 1. *Typical laser beam machining system*

surfaces were examined using a digital microscope. The edges of grooves and blind holes were straight, burr-free, and regular in two different types of materials. Neither material had a heat-affected zone. The water-conducting laser processing technique was practicable, according to experiments on precision metal machining. Yongfei et al. [10] examined how different settings of Water Guided Laser Machining (WGLM) affected the micro-morphology of materials and the way that lasers interact with materials. During the tests, thin samples of 316L stainless steel were machined with slots and grooves using the WGLM technology. After experiments, the 2D and 3D micro-topography was examined. The results of the studies showed that the machining time and the number of machining times have no effect on the breadth of deposition layers.

The glass material was coated to increase its absorptivity and the impact of coating and the laser machining parameters, such as laser power, laser scanning speed, and angle of inclination of the workpiece on the depth and width of the slot, aspect ratio, and material removal rate (MRR) using a 2k factorial design and analysis of variance (ANOVA) by Posa et al [11]. The depth of the slot increased four times, the breadth of the slot increased twice, and the MRR increased seven times when coated glass work samples were compared to uncoated glass work samples. Demarbaix et al. [12] investigated the effects of laser settings on roughness, local sintering, and machining depth during laser machining of Yttrium Oxide Tetragonal Zirconia Polycrystalline ceramic material. The spot overlap, which was related to the repetition rate and feed rate, was discovered to be a factor in roughness and local sintering. The average power had very little impact on sintering, in contrast to the spot overlap. The optimal settings were determined to be an average power of 15 W, a feed rate of 1100 mm/s, a repetition rate of 15 kHz, and a slice of 5 m. When paired with other process variables, including average power, duty cycle, pulse repetition rate, and scanning speed, Pramanik et al. [13] examined the impact of sawing angle on the diameter deviation of Monel sheet metal. The input parameter sawing angle had a crucial influence in the top and bottom diameter variation when drilling 0.7 mm thick Monel K-500 alloy sheet using a low fibre laser beam. By adjusting the controllable process parameters to achieve the required diameter deviation, the proposed model was found to be valid. Regression analysis was used to create a model that forecasts how different process parameters would affect the quality of laser cuts. The optimization process in this paper used the teaching-learning algorithm. Muthuramalingam et al. [14] optimised the effects of process factors on surface performance measures when milling titanium alloy using a Taguchi-Grey relational technique. They found that laser power significantly affects the quality measurements of surface roughness and taper angle in LBM due to the relevance of plasma energy. The ideal process parameter set of laser power (3 kW), nozzle distance (1.5 mm), focal length (2 mm), and gas pressure (2 bar) was chosen due to its ability to produce reduced plasma energy with a precision of

2.2 %. Lower surface roughness was produced by the reduced nozzle distance and higher laser power due to the formation of micro-craters and decreased particle adhesion. Regression modelling and particle swarm optimization (PSO) were combined in a hybrid technique by Shrivatsava et al. [15] to optimise the process parameters during the laser cutting of Inconel-718 sheet. The trials made use of four machining parameters: cutting speed, laser power, standoff distance, and assist gas pressure. The kerf width and kerf taper were employed as output quality characteristics. The L27 orthogonal array was used to conduct the studies. When the experimental results were contrasted with the ideal outcomes, it became clear that there had been individual improvements in the output quality attributes of kerf width and kerf taper of roughly 10 % and 57 %, respectively. There was an improvement of 46 % in overall performance during the optimization. Also addressed was the effect of various process parameters on performance measures.

Deng et al. [16] attempted a novel material processing in which laser surface melting modification combined with precision milling was done to improve the surface integrity and machinability. The surface modification using a laser was done between 1397 °C and 2000 °C. This process, along with the controlled parametric setting of the precision milling, resulted in the improvement of surface finish by 90.36 % and tool life by 61.03 %. The influence of the CO_2 laser parameters, such as the cutting speed and laser power on the surface roughness parameter of the low-carbon steel was studied using ANOVA by Boujelbene [17]. Boujelbene et al. [18] investigated the effect of laser cutting conditions, such as cutting speed, laser power, and gas pressure on the surface roughness of titanium specimens using the Taguchi method. It was found that surface roughness decreases with faster cutting speeds and increases with the evolution of thermal energy by laser power. The optimum cutting conditions for the minimum value of Ra and Rt were found.

The experimental study conducted by Cekic et al. [19] showed that the surface roughness (*Ra*) value decreases with the use of N_2 as an assist gas and at a higher cutting speed. Kim et al. [20] explored the possibilities to machine AlSiC composites using a hybrid-hybrid system of a combination of ultrasonic and laser-assisted turning processes. The cutting force developed, and the surface roughness of the machined components was comparatively less than that of the conventional machining forces. The surface topography of the machined surface is an interesting parameter in tribology and fluid mechanics for the effective movement and separation of the fluid in the microfluidic chips of the micromechanical systems [20]. As the presence of ceramic particles in the metal matrix composites (MMCs) accelerates tool wear, thus increasing the cutting force developed and surface roughness of the finished components, laser machining and hybrid laser machining are the solutions for this problem [22].

This research on finding the individual and interactive effect of the process parameters on surface roughness of microchannel machined using LBM will be useful in understanding the laser machining of Al/TiB_2 composites, which are used in different applications. Experiments were carried out using a Taguchi L9 orthogonal array, and ANOVA was used to investigate the impact of process factors on surface roughness. The surface roughness of microchannels was measured using an atomic force microscope.

1 MATERIALS AND METHODS

In this study, Al A356 alloy and TiB_2 ceramic particles were selected as the matrix and reinforcement materials for the in-situ synthesis of composite samples. The preparation of the nanocomposite material was done by melting 500 g of aluminium A356 alloy in a carbon crucible at 725 °C with the help of an electric furnace, and a pre-weighed mixture of K_2TiF_6 and KBF_4 salts were added to the melt. Then the melt was raised to a temperature of 800 °C and allowed to undergo aluminothermic reactions for a duration of one hour with intermittent stirring at a regular interval of 10 min. The slag floated on the top surface of the melt was removed, and the composite melt was transferred to a preheated clay graphite crucible for treatment with ultrasonic vibrations of 20.1 kHz frequency. A Ti-6Al-4V sonotrode of 40 mm diameter was employed for the effective transfer of ultrasonic vibrations. The composite melt was cast into a pre-heated mould of a diameter of 18 mm and length of 110 mm. A detailed description of nanocomposite fabrication is discussed in [23] to [25]. The X-Ray diffractograph obtained from the composite samples was indexed with the help of Joint Committee on Powder Diffraction Standards (JCPDS) software; the indexed pattern is presented in Fig. 2a. The indexed pattern presented in Fig. 2a. closely matches the standard pattern of aluminium (JCPDS-No: 040787), Si (JCPDS-No: 271402) and TiB_2 particles (JCPDS-No: 350741). The indexing of the diffractograph confirmed the formation of TiB_2 particles and the absence of any other intermetallic phases and/or slag infusion.

To ensure the formation of TiB_2 particles, a sample of the thickness of 10 mm was cut and analysed using Cu-Kα radiation in a Shimadzu XD-D1 XRD analyser. Further, to analyse the particle size, a small disc of ~500 µm thick nanocomposite sample was sliced and further thinned with help of disc grinding, dimple grinding, and Argon ion milling. The ion-milled nanocomposite disc was analysed using a JEOL JEM 2100 Transmission Electron Microscope (TEM) operated at 200 kV. The TEM micrograph of the ultrasonic treated A356/2TiB_2 composite sample is shown in Fig. 2b, and it confirms that the particles are in the nano-regime (<100 nm) and the average particle size is 29 nm ± 12 nm. The TEM micrograph further confirms that the hexagonal disc-shaped TiB_2 nanoparticles are dispersed uniformly in the α-Al matrix.

The Al/TiB_2 nanocomposite exhibits an average ultimate tensile strength of 290 MPa in as-cast and 330 MPa in T6 conditions. The hardness of the nanocomposite is in the range of 160 VHN to 180 VHN [26] and [27]. The presence of TiB_2 particles in the aluminium matrix impedes the propagation of dislocation through the matrix phases. The resistance to dislocation propagation increases the strength of the composite material and the presence of the reinforcement reduces its plasticity. This property modification in turn increases the cutting force requirement, cutting temperature, and tool wear during conventional machining.

Literature reveals that the presence of nano-sized TiB_2 particles induces abrasive wear on cutting tools due to the scratching effect of hard nano-sized particles [28]. In general, the conventional machining of composite material with TiB_2 particles may result in machining issues such as smearing, micro-scratches, and pits on the machined surfaces. In the case of a spark-machining method like EDM, the presence of nano-sized particles reduces the electrical conductivity of the composite and also adversely affects the debris removal and spark gap. Not only the mechanical property-related challenges but also the physical property challenges and process difficulties makes Al/TiB_2 hard to machine. LBM is more preferable for

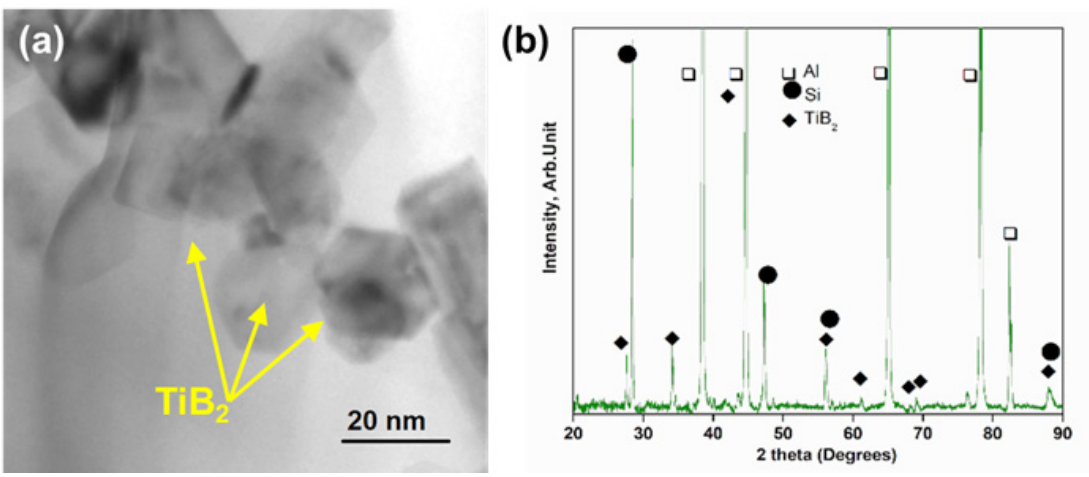

Fig. 2. *a) Bright field TEM microstructure, and b) X-ray diffraction (XRD) pattern of A356/2TiB2 composite sample*

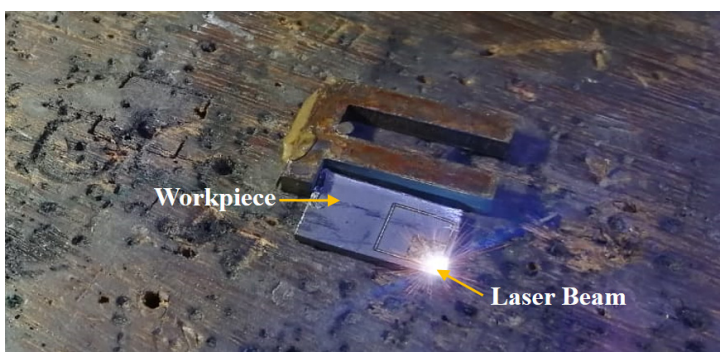

Fig. 3. *Laser machining of the workpiece material*

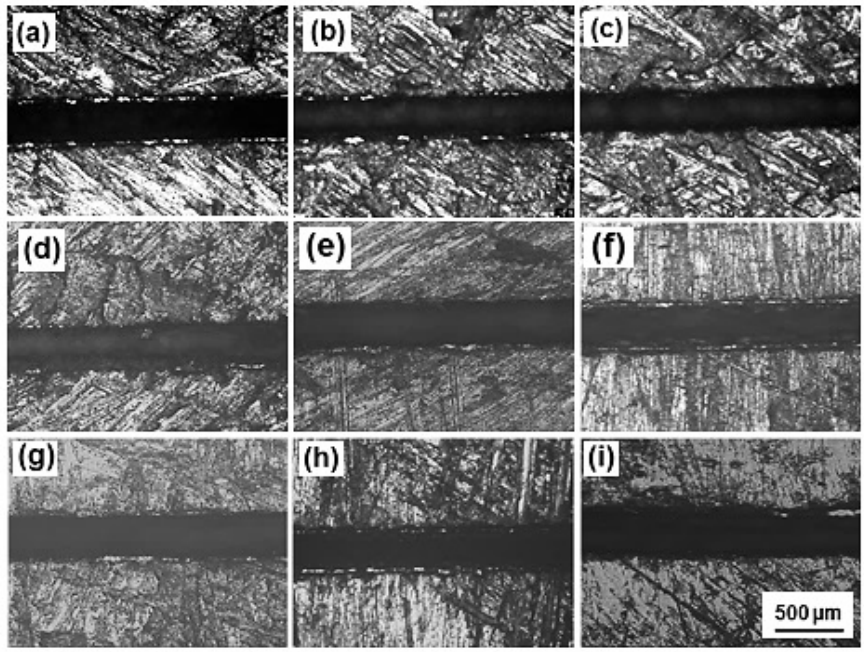

Fig. 4. *Top view of the microchannels obtained for various combinations of LBM parameters; a) experiment 1, b) experiment 2, c) experiment 3, d) experiment 4, e) experiment 5, f) experiment 6, g) experiment 7, h) experiment 8, and i) experiment 9*

generating micro-features with low material removal, high accuracy in dimension, and good surface finish. The heating source in this noncontact machining process is used to heat, melt, and vaporize the material from the work pieces. The advantages of this process are the absence of tool wear, no force exerted on the workpiece, fast processing, and precision machining. Therefore, LBM is chosen for machining microchannels in Al/TiB_2 composite.

Microchannels were machined on the nano-composite samples using the Nd: YAG Q switched laser beam machining system made by Lee Lasers, USA. This laser machine uses argon as the assist gas that passes coaxially with the laser beam through a conical nozzle. The parameters including nozzle diameter, focal length of the lens, and nozzle stand-off distance were all kept constant during the experiments. Laser machining of the workpiece material is shown in Fig. 3.

The input process parameters that were varied while conducting the experiments are laser power, frequency, assist gas pressure, and cutting speed. The input process parameters and their levels are given in Table 1.

2 RESULTS

The bright field optical micrograph of the microchannels machined using LBM is shown in Fig. 4 and the cross-sectional view of the same are shown in Fig. 5. This microscope is a polarized light microscope with a charge-coupled device (CCD) camera and has a magnification in the range of 100× to 1000×.

Table 1. *Input process parameters and their levels*

Factor	Designation of input parameters	Level		
		1	2	3
Power [kW]	A	5	7	9
Frequency [kHz]	B	3	4	5
Gas pressure [bar]	C	2	4	6
Cutting speed [mm/min]	D	100	150	200

The laser beam machined microchannels were examined using an atomic force microscope (AFM) to obtain the profile and value of surface roughness. The surface roughness profile images are shown in Fig. 6.

Taguchi's standard orthogonal array (OA) was used to establish the experimental design of a combination of process parameters [29]. The quality loss function used in these experiments is based on "the smaller the better" as the objective of this

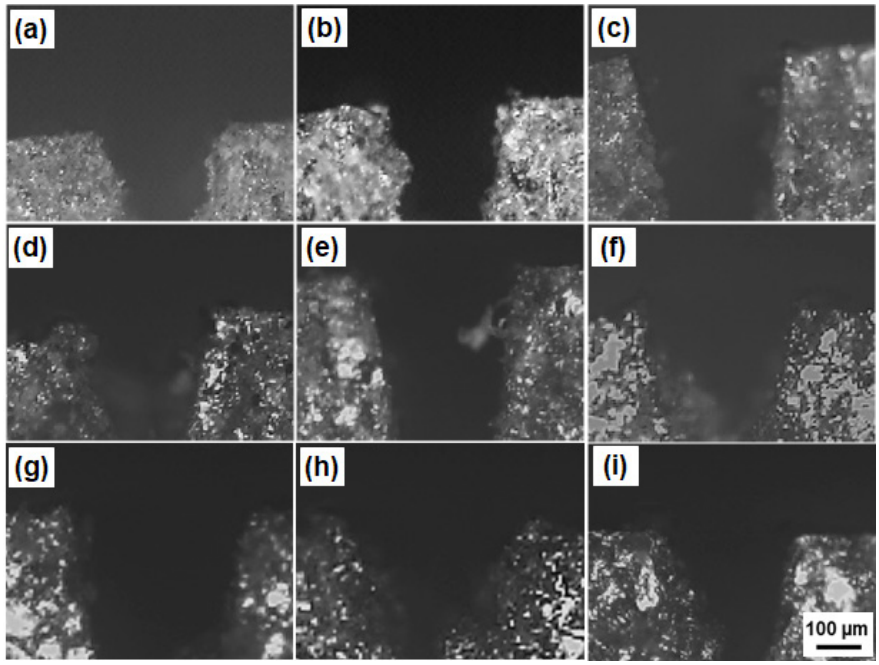

Fig. 5. *Cross-sectional view of microchannels obtained for various combinations of LBM parameters; a) experiment 1, b) experiment 2, c) experiment 3, d) experiment 4, e) experiment 5, f) experiment 6, g) experiment 7, h) experiment 8, and i) experiment 9*

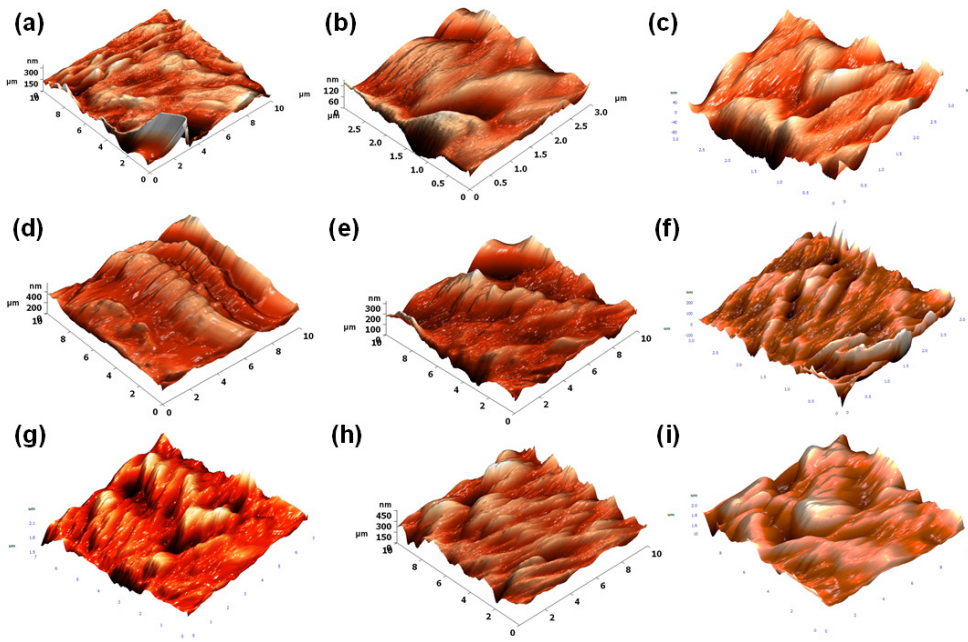

Fig. 6. Surface roughness image of microchannels measured using the AFM; *a) experiment 1, b) experiment 2, c) experiment 3, d) experiment 4, e) experiment 5, f) experiment 6, g) experiment 7, h) experiment 8, and i) experiment 9*

work is to obtain minimum surface roughness of microchannels. The experimental combination of machining parameters and response value (surface roughness) achieved are given in Table 2. The L9 experimental values were statistically examined using the Minitab software based on Taguchi's methodology. A regression equation was obtained for the data to determine the relationship between the input process parameters and the response parameter surface roughness (*Ra*), which is given in Eq. (1).

$$Ra = 349 - 52.9\,A - 81.6\,B - 41.0\,C + 0.329\,D + 10.86\,AB + 4.97\,AC + 3.18\,BC. \quad (1)$$

The predicted values of surface roughness Ra were obtained using Eq. (1) are shown in Table 2. The very low percentage error between the predicted and experimental values of Ra shown in this table indicates the high reliability of the experimental data.

2.1 Analysis of Variance (ANOVA) for Surface Roughness

The following Table 3 shows the ANOVA calculations for surface roughness. The percentage contribution in this table shows that the laser power influences surface roughness to the maximum extent and is then followed by other parameters, such as cutting speed, frequency, and gas pressure. The effect of interaction between the process parameters on *Ra* in the descending order of their effect is power × frequency, power × gas pressure, and frequency × gas pressure. The statistical analysis yielded an R^2 value of 95.13 %, which shows the high accuracy of the experimental data.

2.2. Main Effect Plot for Means for Surface Roughness

The main effect plot for means for surface roughness obtained through the statistical analysis shown in Fig. 7. which shows that the minimum surface roughness of the microchannel is obtained at Level 3 of cutting speed (200 mm/min), Level 1 of gas pressure (2 bar), Level 2 of frequency (4 kHz) and Level 1 (5 kW) of laser power. The main effect plots for means show the trend of the influence of the individual input process parameters on surface roughness. The surface roughness is also influenced by the effect of interaction between the input process parameters also. Thus, the contour plots were obtained for this purpose and the effect of the interaction of two process parameters on surface roughness when the other input parameters are kept constant at their optimum level was studied.

2.3 Contour Plots and Parametric Studies for Surface Roughness

The contour plots shown in Fig. 8 are used to study the influence of interaction between the input process parameters on surface roughness (*Ra*). The effect of interaction between cutting speed and pulse frequency

Table 2. *Experimental combination of machining parameters, experimental and predicted values of Ra and error in percentage*

Experiment number	Input parameter				Response value [nm]		Error [%]
	A	B	C	D	Surface roughness		
					Experiment	Predicted	
1	5	3	2	100	21.5	22.28	0.035
2	5	4	4	150	11.23	10.93	0.027
3	5	5	6	200	11.76	12.3	0.044
4	7	3	4	200	40.67	41.08	0.010
5	7	4	6	100	27.98	28.34	0.013
6	7	5	2	150	18.89	19.53	0.033
7	9	3	6	150	51.75	50.29	0.029
8	9	4	2	200	37.63	36.16	0.065
9	9	5	4	100	67.403	65.02	0.037

Table 3. *Results of ANOVA for Ra*

Source	Degrees of freedom	Sum of squares	% Contribution	F-Value	P-Value
Regression	7	5761.32	95.13	2.06	0.0491
Power	1	3904.61	67.96	1.40	0.0946
Frequency	1	23.19	1.70	1.76	0.0411
Gas pressure	1	161.43	1.04	1.33	0.155
Cutting speed	1	401.56	4.11	1.25	0.0464
Power × Frequency	1	426.07	11.93	1.03	0.0495
Power × Gas pressure	1	644.85	6.66	2.12	0.383
Frequency × Gas pressure	1	199.61	1.71	0.50	0.0608
Error	1	398.73	4.87		

on *Ra* is shown in Fig. 8 a. The region is found between Levels 1 and 2 of frequency and Level 1 of cutting speed and between Levels 2 and 3 of frequency and Levels 2 and 3 of cutting speed. The minimum region for surface roughness is obtained for the combination of high pulse frequency × high cutting speed and for low pulse frequency × low cutting speed. In the pulsed mode laser cutting, the extent of spot overlap influences the surface roughness. The combination of pulse frequency and cutting speed mainly decides the extent of spot overlap. The greater the spot overlap, the smoother the cut edge surface will be. The above combinations result in a high level of spot overlapping and continuous power density per unit length, which gives complete cutting with a uniform smooth surface. The influence of the interaction effect of laser power and cutting speed on *Ra* is shown in Fig. 8b. The region that yields minimum *Ra* is Levels 1 and 2 of laser power and all the levels of cutting speed. According to the results of the study, a medium level of laser power combined with high cutting speed generates a surface with minimum surface roughness. This combination provides just sufficient time of exposure of the work material to the laser.

The influence of the interaction effect of cutting speed and gas pressure on *Ra* is shown in Fig. 8c. The levels that yield minimum surface roughness is Level 1 of gas pressure and level 2 of cutting speed. The combination of low gas pressure and medium cutting speed leads to minimum surface roughness. Medium cutting speed provides adequate exposure of the work material to the laser, and minimum gas

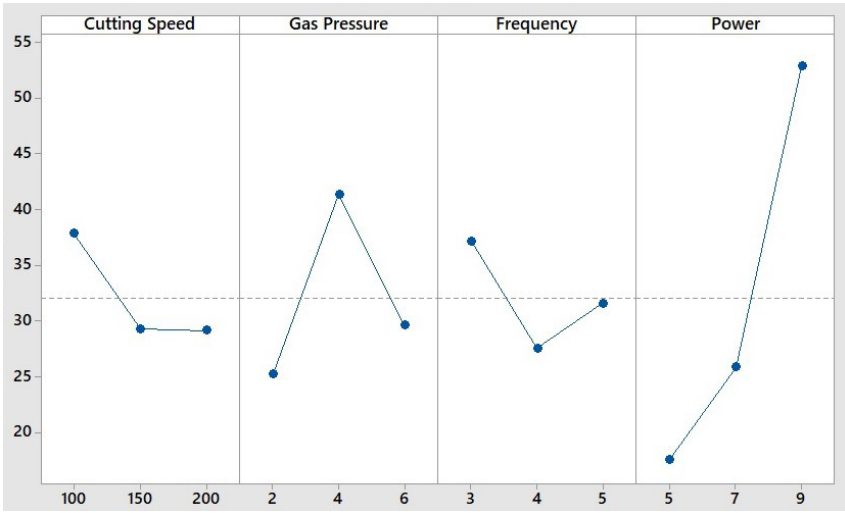

Fig. 7. *Main effect plots for means - Input process parameters vs. surface roughness (Ra)*

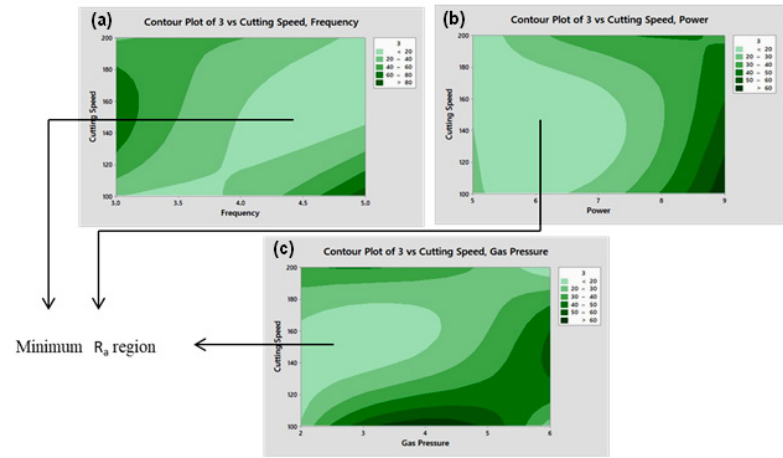

Fig. 8. *Contour Plots for a) Ra vs. cutting speed × pulse frequency, b) Ra vs. laser power × cutting speed, and c) Ra vs. cutting speed × gas pressure*

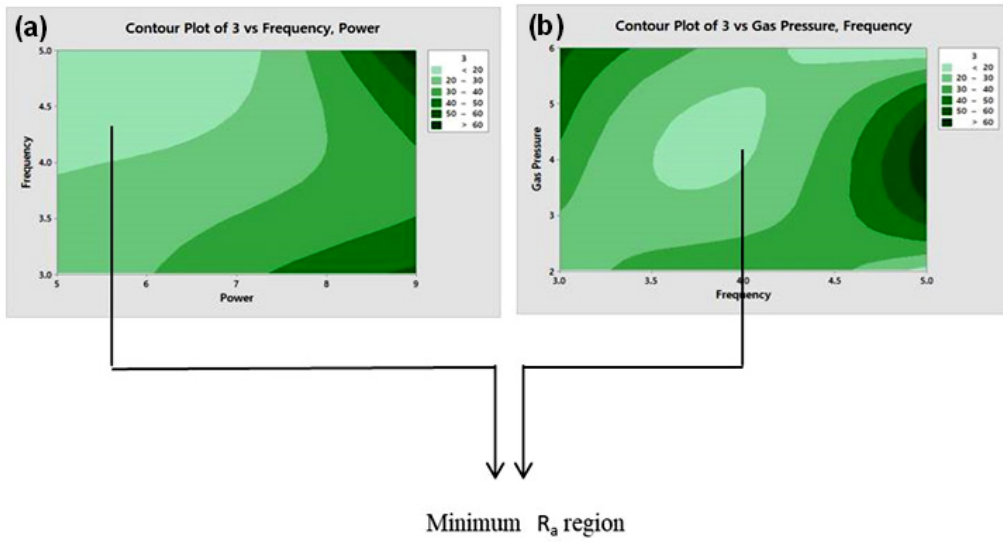

Fig. 9. *Contour plots for a) Ra vs. Pulse frequency × Laser power, and b) Ra vs. Gas pressure × Pulse frequency*

pressure prevents the solidification of the material in the channel itself. This improves the surface finish of the microchannel.

Fig. 9a show the effect of the interaction between pulse frequency and laser power on *Ra*. The region that yields minimum *Ra* is found between Levels 2 and 3 of pulse frequency and Levels 1 and 2 of laser power. Moderate laser power with high frequency allows for an adequate amount of exposure of the work material to the laser for ablation and thus provides minimum roughness on the machined surface. The influence of the interaction effect of gas pressure and pulse frequency on *Ra* is shown in Fig. 9b. The levels that yield minimum *Ra* are found between Levels 1 and 2 of gas pressure and Level 3 of pulse frequency. Moderate gas pressure combined with high frequency also leads to an adequate amount of exposure of the work material to the laser thus producing minimum surface roughness.

3 CONCLUSIONS

Experimental investigations were performed to study the influence of laser machining parameters on the surface roughness of microchannels on Al/TiB_2 composite. Laser machining is an excellent choice for machining micro-features on advanced composite materials like Al/TiB_2. The important findings of the work are summarised as follows.

The surface roughness images of the microchannels obtained using the atomic force microscope revealed that the laser micromachining of Al/TiB_2 composite resulted in surface roughness values ranging from 11.23 nm to 67.403 nm. The main effect plots for means show the optimum combination of laser machining parameters to produce a minimum surface roughness value are a cutting speed of 200 mm/min, a gas pressure of 2 bar, a frequency of 4 kHz, and a laser power of 5 kW. The effect of input process parameters on Ra in the descending order of their influence is laser power, cutting speed, frequency, and gas pressure.

Although the main effect plots for means show the trend of the influence of the individual input process parameters on surface roughness, the output process parameter is also influenced by the effect of interaction between the input process parameters. Thus, contour plots were obtained for this purpose, and the effect of the interaction of two process parameters on surface roughness when the other input parameters are kept constant at their optimum level was studied.

The effect of interaction between the input process parameters on Ra in the descending order of their influence is power × frequency, power × gas pressure, and frequency × gas pressure.

4 ACKNOWLEDGEMENTS

The authors thank the management of PSG College of Technology, Coimbatore, for their financial support in conducting experiments.

5 REFERENCES

[1] Dhupal, D., Doloi, B., Bhattacharyya, B. (2008). Pulsed Nd: YAG laser turning of micro-groove on aluminum oxide ceramic (Al2O3). International Journal of Machine Tools and Manufacture, vol. 48, no. 2, p. 236-248, **DOI:10.1016/j.ijmachtools.2007.08.016**.

[2] Khot Rahul, S., Venkateshwara Rao, T., Harshad, N., Girish, H., Ishigaki, T., Madhusudan, P. (2021). An Investigation on Laser Welding Parameters on the Strength of TRIP Steel. *Strojniški vestnik - Journal of Mechanical Engineering*, vol. 67 no. 1-2, p. 45-52, **DOI:10.5545/sv-jme.2020.6912**.

[3] Li, L. (1994). Three-dimensional laser micromachining. *Microelectronics Technology and Process Integration*, vol. 2335, p. 212-220, **DOI:10.1117/12.186058**.

[4] Gower, M.C. (1998). Industrial applications of pulsed lasers to materials microprocessing. *High-Power Laser Ablation*, vol. 3343, p. 171-182, **DOI:10.1117/12.321564**.

[5] Holmes, A.S. (2001). Laser fabrication and assembly processes for MEMS. *Laser Applications in Microelectronic and Optoelectronic Manufacturing VI*, vol. 4274, p. 297-306, **DOI:10.1117/12.432522**.

[6] Kibria, G., Doloi, B., Bhattacharyya, B. (2014). Investigation into the effect of overlap factors and process parameters on surface roughness and machined depth during micro-turning process with Nd: YAG laser. *Optics & Laser Technology*, vol. 60, p. 90-98, **DOI:10.1016/j.optlastec.2014.01.009**.

[7] Yue, T.M., Lau, W.S. (1996). Pulsed Nd: YAG laser cutting of Al/Li/SiC metal matrix composites. *Material and Manufacturing Process*, vol. 11, no. 1, p. 17-29, **DOI:10.1080/10426919608947458**.

[8] Qiao, H., Zhihe, C., Jianfeng, C., Zhao, J. (2021). Experimental study on water jet guided laser micro-machining of mono-crystalline silicon. *Optics & Laser Technology*, vol. 140, art. ID 107057, **DOI:10.1016/j.optlastec.2021.107057**.

[9] Cao Z.H., Qiao, H.C., Zhao, J.B. (2020). Experimental study on laser water-jet machining of metal material. *Opto-Electronic Engineering*, vol. 47, no. 2, p. 190423-1, DOI:10.12086/oee.2020.190423. (in Chinese)

[10] Yu, Y.F., Qiao, H.C, Cao, Z.H., Zhao, J.B., Zhang, Y.N., Wu, J.J. (2020). Effect of water-guided laser machining technology on micro-morphology of 316L stainless steel. *Opto-Electronic Engineering*, vol. 47, no. 11, p. 190654-1, **DOI:10.12086/oee.2020.190654**. (in Chinese)

[11] Posa, V., Vardhan, M., Sundaram, (2021). Experimental study of micromachining on borosilicate glass using CO_2 laser. Journal of Manufacturing Science and Engineering, vol. 143, no. 5, art. ID.051007, **DOI:10.1115/1.4048639**.

[12] Demarbaix, A., Ducobu, F., Juste, E., Petit, F., Duterte, C., Rivière-Lorphèvre, E. (2021). Experimental investigation on green ceramic machining with nanosecond laser source. *Journal of Manufacturing Processes*, vol. 61, p. 245-253, **DOI:10.1016/j.jmapro.2020.11.031**.

[13] Pramanik, D., Kuar, A.S., Sarkar, S., Mitra, S. (2020). Evaluation of sawing approach of hole quality characteristics in low power fiber laser trepan drilling of monel k-500 superalloy sheet. *Optik*, vol. 224, art. ID 165642, **DOI:10.1016/j.ijleo.2020.165642**.

[14] Muthuramalingam, T., Akash, R., Krishnan, S., Phan, N.H., Pi, V.N., Elsheikh, A.H. (2021). Surface quality measures analysis and optimization on machining titanium alloy using CO_2 based laser beam drilling process. *Journal of Manufacturing Processes*, vol. 62, p. 1-6, **DOI:10.1016/j.jmapro.2020.12.008**.

[15] Shrivastava, P.K., Pandey, A.K. (2018). Optimization of machining parameter during the laser cutting of Inconel-718 sheet using regression analysis based particle swarm optimization method. *Materials Today: Proceedings*, vol. 5, no. 11, p. 24167-24176, **DOI:10.1016/j.matpr.2018.10.211**.

[16] Deng, B., Peng, F., Zhou, L., Yan, R., Wang, H., Yang, M. (2021). Study on the surface layer formation of aluminum matrix composites and associated machinability in precision milling based on laser melting modification. *Journal of Manufacturing Processes*, vol. 62, p. 670-684, **DOI:10.1016/j.jmapro.2020.12.071**.

[17] Boujelbene, M. (2018). Influence of the CO_2 laser cutting process parameters on the quadratic mean roughness Rq of the low carbon steel. *Procedia Manufacturing*, vol. 20, p. 259-264, **DOI:10.1016/j.promfg.2018.02.038**.

[18] Boujelbene, M., El Aoud, B., Bayraktar, E., Elbadawi, I., Chaudhry, I., Khaliq, A., Elleuch, Z. (2021). Effect of cutting conditions on surface roughness of machined parts in CO_2 laser cutting of pure titanium. *Materials Today: Proceedings*, vol. 44, p. 2080-2086, **DOI:10.1016/j.matpr.2020.12.179**.

[19] Cekic, A., Begic-Hajdarevic, D., Kulenovic, M., Omerspahic, A. (2014). CO_2 laser cutting of alloy steels using N_2 assist gas. *Procedia Engineering*, vol. 69, p. 310-315, **DOI:10.1016/j.proeng.2014.02.237**.

[20] Kim, J., Zani, L., Abdul-Kadir, A., Jones, L., Roy, A., Zhao, L., Silberschmidt, V.V. (2022). Hybrid-hybrid machining of SiC-reinforced aluminium metal matrix composite. *Manufacturing Letters*, vol. 32, p. 63-66, **DOI:10.1016/j.mfglet.2022.04.002**.

[21] Bahrami, M., Yovanovich, M.M., Culham, J.R. (2006). Pressure drop of fully developed, laminar flow in rough microtubes, *Journal of Fluids Engineering*, vol. 128, no. 3, p. 632-637, **DOI:10.1115/1.2175171**.

[22] Chen, J.P., Gu, L., He, G.J. (2020). A review on conventional and nonconventional machining of SiC particle-reinforced aluminium matrix composites. *Advances in Manufacturing*, vol. 8, p. 279-315, **DOI:10.1007/s40436-020-00313-2**.

[23] Nampoothiri, J., Harini, R.S., Nayak, S.K., Raj, B., Ravi, K.R. (2016). Post in-situ reaction ultrasonic treatment for generation of Al-4.4 Cu/TiB_2 nanocomposite: A route to enhance the strength of metal matrix nanocomposites. *Journal of Alloys and Compounds*, vol. 683, p. 370-378, **DOI:10.1016/j.jallcom.2016.05.067**.

[24] Nampoothiri, J., Raj, B., Ravi, K.R. (2015). Role of ultrasonic treatment on microstructural evolution in A356/TiB_2 in-situ composite. *Transactions of the Indian Institute of Metals*, vol. 68, p. 1101-1106, **DOI:10.1007/s12666-015-0653-2**.

[25] Nampoothiri, J., Balasundar, I., Raghu, T., Ravi, K. R. (2020). Structural and mechanical behavior of Al-4.4 Cu/2TiB_2 in-situ nanocomposites fabricated by post-in-situ reaction ultrasonic processing. *Metallurgical and Materials Transactions B*, vol. 51, p. 149-160, **DOI:10.1007/s11663-019-01713-x**.

[26] Mandal, A., Chakraborty, M., Murty, B.S. (2008). Ageing behaviour of A356 alloy reinforced with in-situ formed TiB2

particles. Materials Science and Engineering: A, vol. 489, no. 1-2, p. 220-226, **DOI:10.1016/j.msea.2008.01.042**.

[27] Kumar, S.D., Mandal, A., Chakraborty, M., (2015). On the age hardening behavior of thixoformed A356-5TiB_2 in-situ composite. *Materials Science and Engineering: A*, vol. 636, p. 254-262, **DOI:10.1016/j.msea.2015.03.076**.

[28] Chen, J. Yu, W., Zou, Z., Li, Z., Chen, D., An, Q., Geng, J., Chen, M., Wang, H. (2021). Effects of in-situ TiB2 particles on machinability and surface integrity in milling of TiB2/2024 and TiB2/7075 Al composites. *Chinese Journal of Aeronautics*, vol. 34, no. 6, p. 110-124, **DOI:10.1016/j.cja.2020.06.017**.

[29] Ross, P.J. (1988) *Taguchi Techniques for Quality Engineering*. McGraw Hill, New York.